pp. 1–23 (2022)

A finite element scheme for the numerical solution of the Navier–Stokes/Biot coupled problem

A. Lozovskiy*, M. A. Olshanskii†, and Yu. V. Vassilevski*‡§

Abstract — A finite element method for a monolithic quasi-Lagrangian formulation of a fluid–porous structure interaction problem with a corrected balance of stresses on the fluid–structure interface is considered. Deformations of the elastic medium are not necessarily small and are modelled using Saint Venant–Kirchhoff (SVK) constitutive relation. The stability of the method is proved in a form of energy bound for the finite element solution.

Keywords: Fluid-structure interaction, semi-implicit scheme, monolithic approach, blood flow, numerical stability, finite element method

MSC 2010: 76M10, 65M12, 74F10, 76Z05

Blood flow in a vessel with permeable walls or penetration of oil through a crack in a porous matrix can be seen as the interaction of a freely flowing fluid with a fluid-saturated poroelastic structure. A continuum mechanics description of such fluid-poroelastic phenomena often leads to coupled systems of (Navier–)Stokes and Biot equations [25, 35]. Recently, there has been a growing interest in the numerical solution of the Stokes–Biot and Navier–Stokes–Biot problems. Several authors suggested solution strategies based on decomposition of the system into fluid and poroelastic loosely coupled problems to allow for computationally efficient time-stepping schemes [5, 8]. For the reason of better stability, monolithic methods for the (Navier–)Stokes–Biot equations have become popular in the literature. They differ in the form of equations and the numerical treatment of the coupling conditions on the interface between a free flow domain and a domain occupied by the porous structure. In [2] the continuity of fluid fluxes on the interface is imposed weakly with the help of a Lagrange multiplier and in [36] an interior penalty discontinuous Galerkin method is applied to obtain a discrete coupled formulation. The Nitsche approach is used for coupling fluid and poroelastic finite element formula-

*Marchuk Institute of Numerical Mathematics, RAS, Moscow 119333, Russia

†Department of Mathematics, University of Houston, Houston, TX 77204

‡Sechenov University, Moscow 119991, Russia

§Sirius University, Sochi 354340, Russia.

E-mails: alex.v.lozovskiy@gmail.com, maolshanskiy@uh.edu, yuri.vassilevski@gmail.com

The research of the first author was supported by the Russian Science Foundation grant 19-71-10094.

tions in [1, 9]. Combination of the Nitsche approach and unfitted finite elements [1] adds extra flexibility to the numerical solution.

Many publications on numerical methods for the fluid–poroelastic problem ignore inertia effect in the fluid and formulate the free fluid problem as a Stokes system. One reason for such simplification is the lack of the energy dissipation principle for the Navier–Stokes–Biot problem with the common interface conditions, which hinders the analysis in this case. This issue is well known already for the Navier–Stokes–Darcy (the Navier–Stokes–Biot problem with a rigid structure), where a local well-posedness of the system is currently known only under a smallness assumption (even in 2D) and the proof uses involved arguments that work in the absence of *a priori* energy bound [4, 20]. In the context of the Navier–Stokes/Darcy coupling the issue was addressed in [10, 11], where interface conditions were modified to ensure the thermodynamic consistency of the complete system. In the present report, we follow [10, 11] and employ the suggested correction to the stress balance in the Navier–Stokes–Biot to end up with a dissipative system and a stable numerical method. A common simplification we avoid is the assumption that deformations of poroelastic structure are small enough not to affect the free fluid flow. This assumption is plausible in certain cases and allows to extend numerical analysis well-known for fluid equations in a fixed given domain to the (Navier–)Stokes/Biot coupled system (see, e.g., [34]). However, in other situations, e.g., in poroelastic models of living cells [32] or blood clots [33], the deformations can be large enough and dynamic. Therefore, in this work we account for time dependent deformations in the definition of flow domain and accommodate finite elastic strains by using the SVK elasticity model.

We consider an arbitrary Lagrangian–Eulerian (ALE) formulation of the Navier–Stokes–Biot system and further introduce a monolithic finite element method. Our finite element method features the formulation of all equations in the reference coordinates encoding all information on geometry deformation in solution-dependent coefficients. This formulation allows a simple application of the method of lines for the time discretization. Such monolithic approach was proved to be efficient for fluid–structure interaction (FSI) problems with an impermeable elastic structure [23, 29, 30], and we extend it here to the case of poroelasticity. In the spirit of monolithic formulations, we apply here the same finite elements to approximate fluid velocity and pressure in both domains. We choose the Taylor–Hood element (P2-P1) for this purpose, which is a valid Darcy element for applications where the local mass conservation is not critical [24]. We use the same P2 element for the structure velocity. To enforce the continuity of fluid flux through the interface, we use the penalty approach (the Nitsche approach as in [1] would be an alternative).

The remainder of the paper is organized in four sections. We formulate the governing equations, interface and boundary conditions in Section 1. The same section presents the integral formulation, the energy balance of the system, and an ALE formulation that we use for the discretization. The finite element method is introduced in Section 2 and its numerical stability is proved in Section 3. Section 4 presents the results of several numerical experiments.

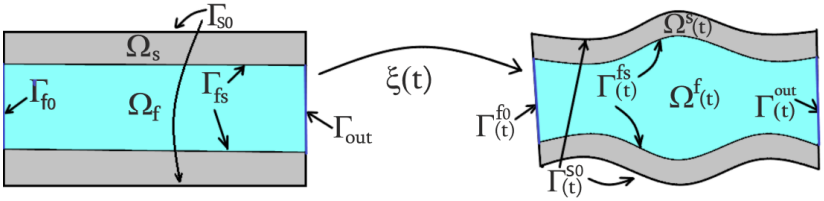

Figure 1. Reference and physical domains and boundaries.

1. FPSI model

Let us consider a time-dependent domain $\Omega(t) \subset \mathbb{R}^3$ containing fluid and an elastic porous structure. A subdomain $\Omega^f(t)$ is entirely occupied by fluid and a subdomain $\Omega^s(t)$ is occupied by porous elastic solid fully saturated with fluid. These subdomains are non-overlapping and $\overline{\Omega(t)} = \overline{\Omega^f(t)} \cup \overline{\Omega^s(t)}$. Two regions are separated by the interface $\Gamma^{fs}(t) := \partial\Omega^f(t) \cap \partial\Omega^s(t)$.

In the present paper, the equations governing the fluid and solid motion will be written in the reference domains

$$\Omega_f = \Omega^f(0), \quad \Omega_s = \Omega^s(0), \quad \Gamma_{fs} = \Gamma^{fs}(0).$$

The deformation of the poroelastic part is given by the mapping

$$\xi_s \ : \ \Omega_s \times [0,T] \to \bigcup_{t\in[0,T]} \Omega^s(t)$$

with the corresponding displacement $\mathbf{u}_s$, $\mathbf{u}_s(\mathbf{x},t) := \xi_s(\mathbf{x},t) - \mathbf{x}$ and *the velocity of the elastic structure* $\mathbf{v}_s = \partial_t \mathbf{u}_s = \partial_t \xi_s(\mathbf{x},t)$.

The fluid dynamics is described by the velocity vector field $\mathbf{v}_f(\mathbf{x},t)$ and the pressure function $p(\mathbf{x},t)$ defined in the whole volume $\Omega(t)$ for all $t \in [0,T]$. Following [5, 25] we represent $\mathbf{v}_f$ in the poroelastic domain through the velocity of structure and the filtration flux $\mathbf{q} = \varphi(\mathbf{v}_f - \mathbf{v}_s)$, where φ is the known porosity coefficient. We denote the fluid pressure in the poroelastic domain by p_d, to emphasize its impact on the Darcy filtration, and in the fluid domain by p_f.

Denote by ρ_s and ρ_f the densities of solid and fluid. Then $\rho_p = \rho_s(1-\varphi) + \rho_f\varphi$ is the density of the saturated porous medium. Denote by σ_s, σ_f the Cauchy stress tensors in porous medium and fluid, respectively. The poroelastic stress tensor is given by $\sigma_p = \sigma_s - \alpha p\mathbf{I}$, where $\alpha > 0$ is Biot's coefficient (typically $\alpha \simeq 1$, so further we set $\alpha = 1$). The porous medium is also characterized by its permeability tensor K. The Biot system in the porous domain and the Navier–Stokes equations in the fluid domain follow from the momenta balance and mass conservation prin-

ciples:

$$\begin{cases} \rho_p \dot{\mathbf{v}}_s + \rho_f \dot{\mathbf{q}} = \operatorname{div} \sigma_p \\ \rho_f \dot{\mathbf{v}}_s + \dfrac{\rho_f}{\varphi} \dot{\mathbf{q}} = -(K^{-1}\mathbf{q} + \nabla p_d) \quad \text{in } \Omega^s(t) \\ -s_0 \dot{p}_d = \operatorname{div}(\mathbf{v}_s + \mathbf{q}) \\ \begin{cases} \rho_f \dot{\mathbf{v}}_f = \operatorname{div} \sigma_f \\ \operatorname{div} \mathbf{v}_f = 0 \end{cases} \quad \text{in } \Omega^f(t) \end{cases} \tag{1.1}$$

where $1/s_0$ is Biot modulus or mixture compressibility modulus, and $\dot{f}$ is the material derivative of quantity f.

We divide the boundary of $\Omega(t)$ into the external boundary of the poroelastic structure $\Gamma^{s0}(t) := \partial\Omega(t) \cap \partial\Omega^s(t)$, fluid Dirichlet and outflow boundaries: $\partial\Omega(t) \cap \partial\Omega^f(t) = \Gamma^{f0}(t) \cup \Gamma^{\text{out}}(t)$ (see Fig. 1). The governing equations are complemented with boundary conditions

$$\mathbf{v}^f = \mathbf{g} \ \text{ on } \Gamma^{f0}(t), \quad \sigma_f \mathbf{n} = \mathbf{0} \ \text{ on } \Gamma^{\text{out}}(t), \quad \sigma_p \mathbf{n} = \mathbf{0} \ \text{ on } \Gamma^{s0}(t), \quad p_d = 0 \ \text{ on } \Gamma^{s0}(t) \tag{1.2}$$

and suitable initial conditions. Instead of $p_d = 0$ we may consider condition on the Darcy flux $\mathbf{q} \cdot \mathbf{n}$ on entire $\Gamma^{s0}(t)$ or its part.

We now discuss coupling conditions on the interface between the fluid and poroelastic domains. Denote by $\mathbf{n}$ the normal vector on $\Gamma^{fs}(t)$ pointing from the fluid to the poroelastic structure. The balance of normal stresses on $\Gamma^{fs}(t)$ is commonly written in terms of the interface conditions: $\sigma_f \mathbf{n} = \sigma_p \mathbf{n}$ and $\mathbf{n}^T \sigma_f \mathbf{n} = -p_d$. This coupling, however, is not known to provide an energy consistent (dissipative) system. For the pure Navier–Stokes/Darcy coupling a remedy was suggested in [10, 12] where the second condition was changed to include a contribution of the fluid kinetic energy. In this paper, we use the same modification in the poroelasticity context and two interface conditions read:

$$\sigma_f \mathbf{n} = \sigma_p \mathbf{n}, \qquad \mathbf{n}^T \sigma_f \mathbf{n} = -p_d + \frac{\rho_f}{2} |\mathbf{v}_f|^2 \quad \text{on } \Gamma^{fs}(t). \tag{1.3}$$

Such modification of the stress balance is similar to modifications of outflow boundary conditions and 1D–3D models coupling conditions in computational fluid dynamics (see, e.g., [6, 7]). The continuity of the normal flux on the fluid-structure interface gives

$$\mathbf{v}_f \cdot \mathbf{n} = (\mathbf{v}_s + \mathbf{q}) \cdot \mathbf{n} \quad \text{on } \Gamma^{fs}(t). \tag{1.4}$$

Finally, the Beavers–Joseph–Saffman condition sets the tangential component of the normal stress proportional to the fluid 'slip' rate along the interface:

$$\mathbf{P} \sigma_f \mathbf{n} = -\gamma \mathbf{P} K^{-1/2} (\mathbf{v}_f - \mathbf{v}_s) \quad \text{on } \Gamma^{fs}(t) \tag{1.5}$$

where $\mathbf{P}$ is the orthogonal projector on the tangential plane to $\Gamma^{fs}(t)$.

1.1. Integral formulation

In the preparation for the finite element method, we write out an integral formulation of the FPSI problem (1.1)–(1.5). We take the inner product of the elasticity equation in (1.1) with a sufficiently smooth ψ_s, integrate it over $\Omega^s(t)$ and integrate the stress term by parts. This adds up with the first Darcy equation multiplied by a sufficiently smooth ψ_d and integrated over $\Omega^s(t)$ to give

$$\begin{aligned}\int_{\Omega^s(t)} (\rho_p \dot{\mathbf{v}}_s + \rho_f \dot{\mathbf{q}}) \cdot \psi_s + (\rho_f \dot{\mathbf{v}}_s + \frac{\rho_f}{\varphi}\dot{\mathbf{q}} + K^{-1}\mathbf{q}) \cdot \psi_d \,\mathrm{d}x + \int_{\Omega^s(t)} \sigma_p : \nabla \psi_s \,\mathrm{d}x \\ - \int_{\Omega^s(t)} p_d \mathrm{div}\, \psi_d \,\mathrm{d}x + \int_{\Gamma^{fs}(t)} (\sigma_p \mathbf{n}) \cdot \psi_s \,\mathrm{d}s \\ - \int_{\Gamma^{fs}(t)} p_d (\psi_d \cdot \mathbf{n}) \,\mathrm{d}s = 0. \end{aligned} \tag{1.6}$$

Further, the fluid momentum equation in (1.1) is multiplied by a smooth vector function ψ_f. Integrating over $\Omega^f(t)$ and integrating the stress term by parts we obtain

$$\int_{\Omega^f(t)} \rho_f \dot{\mathbf{v}}_f \cdot \psi_f \,\mathrm{d}x + \int_{\Omega^f(t)} \sigma_f : \nabla \psi_f \,\mathrm{d}x - \int_{\Gamma^{fs}(t)} \psi_f^T \sigma_f \mathbf{n} \,\mathrm{d}s = 0. \tag{1.7}$$

We add up boundary terms in (1.6) and (1.7) and use interface conditions (1.3)–(1.5) to reorganize them

$$\begin{aligned}&\int_{\Gamma^{fs}(t)} (\sigma_p \mathbf{n}) \cdot \psi_s \,\mathrm{d}s - \int_{\Gamma^{fs}(t)} p_d (\psi_d \cdot \mathbf{n}) \,\mathrm{d}s - \int_{\Gamma^{fs}(t)} \psi_f^T \sigma_f \mathbf{n} \,\mathrm{d}s \\ &\overset{\text{use (1.3)}}{=} \int_{\Gamma^{fs}(t)} (\sigma_f \mathbf{n}) \cdot (\psi_s - \psi_f) \,\mathrm{d}s - \int_{\Gamma^{fs}(t)} p_d (\psi_d \cdot \mathbf{n}) \,\mathrm{d}s \\ &\overset{\text{split } \sigma\mathbf{n}}{=} \int_{\Gamma^{fs}(t)} (\mathbf{n}^T \sigma_f \mathbf{n})(\psi_s - \psi_f) \cdot \mathbf{n} \,\mathrm{d}s + \int_{\Gamma^{fs}(t)} (\mathbf{P}\sigma_f \mathbf{n}) \cdot \mathbf{P}(\psi_s - \psi_f) \,\mathrm{d}s \\ &\qquad - \int_{\Gamma^{fs}(t)} p_d (\psi_d \cdot \mathbf{n}) \,\mathrm{d}s \\ &\overset{\text{use (1.3),(1.5)}}{=} \int_{\Gamma^{fs}(t)} p_d (\psi_f - \psi_s - \psi_d) \cdot \mathbf{n} \,\mathrm{d}s + \gamma \int_{\Gamma^{fs}(t)} K^{-1/2} \mathbf{P}(\mathbf{v}_f - \mathbf{v}_s) \cdot (\psi_f - \psi_s) \,\mathrm{d}s \\ &\qquad + \int_{\Gamma^{fs}(t)} \frac{\rho_f}{2} |\mathbf{v}_f|^2 (\psi_s - \psi_f) \cdot \mathbf{n} \,\mathrm{d}s. \end{aligned}$$

Summing up (1.6) and (1.7) and using the calculations above we arrive at the integral

equality satisfied by sufficiently smooth FPSI solution $\mathbf{v}_s$, $\mathbf{q}$, $\mathbf{v}_f$, p_d, p_f:

$$\begin{aligned}
&\int_{\Omega^s(t)} \left[(\rho_p \dot{\mathbf{v}}_s + \rho_f \dot{\mathbf{q}}) \cdot \boldsymbol{\psi}_s + (\rho_f \dot{\mathbf{v}}_s + \frac{\rho_f}{\varphi} \dot{\mathbf{q}} + K^{-1}\mathbf{q}) \cdot \boldsymbol{\psi}_d \right] \mathrm{d}x + \int_{\Omega^s(t)} \boldsymbol{\sigma}_p : \nabla \boldsymbol{\psi}_s \, \mathrm{d}x \\
&\quad - \int_{\Omega^s(t)} p_d \mathrm{div}\, \boldsymbol{\psi}_d \, \mathrm{d}x + \int_{\Omega^f(t)} \rho_f \dot{\mathbf{v}}_f \cdot \boldsymbol{\psi}_f \, \mathrm{d}x + \int_{\Omega^f(t)} \boldsymbol{\sigma}_f : \nabla \boldsymbol{\psi}_f \, \mathrm{d}x \\
&\quad + \int_{\Gamma^{fs}(t)} \frac{\rho_f}{2} |\mathbf{v}_f|^2 (\boldsymbol{\psi}_s - \boldsymbol{\psi}_f) \cdot \mathbf{n} \, \mathrm{d}s + \int_{\Gamma^{fs}(t)} p_d (\boldsymbol{\psi}_f - \boldsymbol{\psi}_s - \boldsymbol{\psi}_d) \cdot \mathbf{n} \, \mathrm{d}s \\
&\quad + \gamma \int_{\Gamma^{fs}(t)} K^{-1/2} \mathbf{P}(\mathbf{v}_f - \mathbf{v}_s) \cdot (\boldsymbol{\psi}_f - \boldsymbol{\psi}_s) \, \mathrm{d}s = 0 \qquad (1.8)
\end{aligned}$$

for all sufficiently smooth $\boldsymbol{\psi}_s$, $\boldsymbol{\psi}_d$, and $\boldsymbol{\psi}_f$ such that $\boldsymbol{\psi}_f = \mathbf{0}$ on Γ^{f0}. Equality (1.8) is supplemented by the integral identities that follow from the two continuity equations in (1.1):

$$\int_{\Omega^s(t)} \big(s_0 \dot{p}_d + \mathrm{div}\,(\mathbf{v}_s + \mathbf{q}) \big) q_d \, \mathrm{d}x = 0, \qquad \int_{\Omega^f(t)} q_f \mathrm{div}\, \mathbf{v}_f = 0 \qquad (1.9)$$

for all $q_d \in L^2(\Omega^s(t))$, $q_f \in L^2(\Omega^f(t))$.

To obtain the energy balance identity, we assume that Γ^{f0} and Γ^{out} are steady and $\mathbf{g} = 0$ on Γ^{f0}. We further let $\boldsymbol{\psi}_s = \mathbf{v}_s$, $\boldsymbol{\psi}_d = \mathbf{q}$, $\boldsymbol{\psi}_f = \mathbf{v}_f$ and use $\boldsymbol{\sigma}_p = \boldsymbol{\sigma}_s - p\mathbf{I}$, continuity conditions and (1.4) to arrive at the equality:

$$\begin{aligned}
&\int_{\Omega^s(t)} \left[(\rho_p \dot{\mathbf{v}}_s + \rho_f \dot{\mathbf{q}}) \cdot \mathbf{v}_s + \left(\rho_f \dot{\mathbf{v}}_s + \frac{\rho_f}{\varphi} \dot{\mathbf{q}} \right) \cdot \mathbf{q} + K^{-1} |\mathbf{q}|^2 \right] \mathrm{d}x \\
&\quad + \int_{\Omega^s(t)} \boldsymbol{\sigma}_s : \nabla \boldsymbol{\psi}_s \, \mathrm{d}x + \int_{\Omega^s(t)} s_0 \dot{p}_d p_d \, \mathrm{d}x + \int_{\Omega^f(t)} \rho_f \dot{\mathbf{v}}_f \cdot \mathbf{v}_f \, \mathrm{d}x + \int_{\Omega^f(t)} \boldsymbol{\sigma}_f : \nabla \mathbf{v}_f \, \mathrm{d}x \\
&\quad - \int_{\Gamma^{fs}(t)} \frac{\rho_f}{2} |\mathbf{v}_f|^2 \mathbf{q} \cdot \mathbf{n} \, \mathrm{d}s + \gamma \int_{\Gamma^{fs}(t)} K^{-1/2} |\mathbf{P}(\mathbf{v}_f - \mathbf{v}_s)|^2 \, \mathrm{d}s = 0. \qquad (1.10)
\end{aligned}$$

Using $\boldsymbol{\sigma}_f = \mu_f \mathbf{D}\mathbf{v}_f - p_f \mathbf{I}$, $\mathbf{D}\mathbf{v}_f := (\nabla \mathbf{v}_f + (\nabla \mathbf{v}_f)^T)/2$, $\mathrm{div}\, \mathbf{v}_f = 0$, and rearranging the first two terms by substituting $\rho_p = \rho_s(1-\varphi) + \rho_f \varphi$, we can rewrite the above equality as

$$\begin{aligned}
&\int_{\Omega^s(t)} \left[(1-\varphi)\rho_s \dot{\mathbf{v}}_s \cdot \mathbf{v}_s + \varphi \rho_f \left(\dot{\mathbf{v}}_s + \frac{\dot{\mathbf{q}}}{\varphi} \right) \cdot \left(\mathbf{v}_s + \frac{\mathbf{q}}{\varphi} \right) \right] \mathrm{d}x + \int_{\Omega^s(t)} K^{-1} |\mathbf{q}|^2 \, \mathrm{d}x \\
&\quad + \int_{\Omega^s(t)} \boldsymbol{\sigma}_s : \nabla \boldsymbol{\psi}_s \, \mathrm{d}x + \int_{\Omega^s(t)} s_0 \dot{p}_d p_d \, \mathrm{d}x + \int_{\Omega^f(t)} \rho_f \dot{\mathbf{v}}_f \cdot \mathbf{v}_f \, \mathrm{d}x + \mu_f \int_{\Omega^f(t)} |\mathbf{D}\mathbf{v}_f|^2 \, \mathrm{d}x \\
&\quad - \int_{\Gamma^{fs}(t)} \frac{\rho_f}{2} |\mathbf{v}_f|^2 \mathbf{q} \cdot \mathbf{n} \, \mathrm{d}s + \gamma \int_{\Gamma^{fs}(t)} K^{-1/2} |\mathbf{P}(\mathbf{v}_f - \mathbf{v}_s)|^2 \, \mathrm{d}s = 0. \qquad (1.11)
\end{aligned}$$

The integrals with material derivatives can be readily converted to the variations of kinetic energy by application of the Reynolds transport theorem and recalling that

all parts of $\partial\Omega^f(t)$ are steady except $\Gamma^{fs}(t)$, which normal velocity is $\mathbf{v}_s\cdot\mathbf{n}$:

$$\begin{aligned}
&\frac{\mathrm{d}}{\mathrm{d}t}\frac{1}{2}\int_{\Omega^f(t)}\rho_f|\mathbf{v}_f|^2\,\mathrm{d}x=\int_{\Omega^f(t)}\rho_f\frac{\partial\mathbf{v}_f}{\partial t}\cdot\mathbf{v}_f\,\mathrm{d}s+\frac{1}{2}\int_{\Gamma^{fs}(t)}\rho_f|\mathbf{v}_f|^2\mathbf{v}_s\cdot\mathbf{n}\,\mathrm{d}s\\
&=\int_{\Omega^f(t)}\rho_f\frac{\partial\mathbf{v}_f}{\partial t}\cdot\mathbf{v}_f\,\mathrm{d}s+\frac{1}{2}\int_{\Gamma^{fs}(t)}\rho_f|\mathbf{v}_f|^2\mathbf{v}_f\cdot\mathbf{n}\,\mathrm{d}s-\frac{1}{2}\int_{\Gamma^{fs}(t)}\rho_f|\mathbf{v}_f|^2\mathbf{q}\cdot\mathbf{n}\,\mathrm{d}s\\
&=\int_{\Omega^f(t)}\rho_f\frac{\partial\mathbf{v}_f}{\partial t}\cdot\mathbf{v}_f\,\mathrm{d}s+\frac{1}{2}\int_{\Omega^f(t)}\rho_f\mathrm{div}\,(|\mathbf{v}_f|^2\mathbf{v}_f)\,\mathrm{d}s-\frac{1}{2}\int_{\Gamma^{fs}(t)}\rho_f|\mathbf{v}_f|^2\mathbf{q}\cdot\mathbf{n}\,\mathrm{d}s\\
&\overset{\text{use }\mathrm{div}\,\mathbf{v}_f=0}{=}\int_{\Omega^f(t)}\rho_f\frac{\partial\mathbf{v}_f}{\partial t}\cdot\mathbf{v}_f\,\mathrm{d}s+\int_{\Omega^f(t)}\rho_f((\mathbf{v}_f\cdot\nabla)\mathbf{v}_f)\cdot\mathbf{v}_f\,\mathrm{d}s-\frac{1}{2}\int_{\Gamma^{fs}(t)}\rho_f|\mathbf{v}_f|^2\mathbf{q}\cdot\mathbf{n}\,\mathrm{d}s\\
&=\int_{\Omega^f(t)}\rho_f\dot{\mathbf{v}}_f\cdot\mathbf{v}_f\,\mathrm{d}s-\frac{1}{2}\int_{\Gamma^{fs}(t)}\rho_f|\mathbf{v}_f|^2\mathbf{q}\cdot\mathbf{n}\,\mathrm{d}s.
\end{aligned}$$

We handle the $\Omega^s(t)$-integrals containing material derivatives in (1.11) by the same argument assuming that the elastic structure is incompressible, i.e., $\mathrm{div}\,\mathbf{v}_s=0$, and recalling that the material derivative in the structure is written in the Eulerian terms as $\partial/\partial t+\mathbf{v}_s\cdot\nabla$. Therefore, (1.11) yields

$$\begin{aligned}
&\frac{\mathrm{d}}{\mathrm{d}t}\frac{1}{2}\int_{\Omega^s(t)}\left[(1-\varphi)\rho_s|\mathbf{v}_s|^2+\varphi\rho_f|\mathbf{v}_f|^2\right]\mathrm{d}x+\int_{\Omega^s(t)}K^{-1}|\mathbf{q}|^2\,\mathrm{d}x+\int_{\Omega^s(t)}\boldsymbol{\sigma}_s:\nabla\mathbf{v}_s\,\mathrm{d}x\\
&\quad+\frac{\mathrm{d}}{\mathrm{d}t}\frac{1}{2}\int_{\Omega^s(t)}s_0|p_d|^2\,\mathrm{d}x+\frac{\mathrm{d}}{\mathrm{d}t}\frac{1}{2}\int_{\Omega^f(t)}\rho_f|\mathbf{v}_f|^2\,\mathrm{d}x\\
&\quad+\mu_f\int_{\Omega^f(t)}|\mathbf{D}\mathbf{v}_f|^2\,\mathrm{d}x+\gamma\int_{\Gamma^{fs}(t)}K^{-1/2}|\mathbf{P}(\mathbf{v}_f-\mathbf{v}_s)|^2\,\mathrm{d}s=0
\end{aligned}\tag{1.12}$$

where we used $\mathbf{v}_f=\mathbf{v}_s+\mathbf{q}/\varphi$ in $\Omega^s(t)$ for the brevity. For hyperelastic materials, the work of the elastic stresses represented by $\int_{\Omega^s(t)}\boldsymbol{\sigma}_s:\nabla\mathbf{v}_s\,\mathrm{d}x$, equals the time variation of the strain energy. Therefore, (1.12) shows that the system dissipates the total energy composed of kinetic (the first and the fifth integrals in (1.12)) and free (the third and the fourth integrals in (1.12)) energies. Without the correction in the stress balance on the interface, the sign indefinite term $-\frac{1}{2}\rho_f\int_{\Gamma^{fs}(t)}|\mathbf{v}_f|^2(\mathbf{q}\cdot\mathbf{n})\,\mathrm{d}s$ appears in the energy equality, and the system is not necessarily dissipative.

1.2. ALE formulation

In this paper, we adopt the Arbitrary Lagrangian–Eulerian formulation by extending ξ_s to an auxiliary mapping in the fluid domain

$$\xi_f\ :\ \Omega_f\times[0,T]\to\bigcup_{t\in[0,T]}\Omega^f(t)$$

such that $\xi_s = \xi_f$ on Γ_{fs}, i.e., ξ is globally continuous. In general, ξ_f does not follow material trajectories. Instead, it is defined by a continuous extension of the displacement field to the flow reference domain

$$\mathbf{u}_f := \mathrm{Ext}(\mathbf{u}_s) = \xi_f(\mathbf{x},t) - \mathbf{x} \quad \text{in } \Omega_f \times [0,T]; \quad \mathbf{u} = \begin{cases} \mathbf{u}_s & \text{in } \Omega_s \\ \mathbf{u}_f & \text{in } \Omega_f. \end{cases} \tag{1.13}$$

The corresponding globally defined deformation gradient is $\mathbf{F} = \mathbf{I} + \nabla\mathbf{u}$, and $J := \det(\mathbf{F})$ is its determinant. From now on, for notation simplicity, we will use the same notation for variables defined in the reference configuration as $\mathbf{v}_f(\mathbf{x},t) := \mathbf{v}_f(\xi_f(\mathbf{x},t),t)$ and $p_f(\mathbf{x},t) := p_f(\xi_f(\mathbf{x},t),t)$. We use the notation $\sigma_s \circ \xi_s(\mathbf{x}) := \sigma_s(\xi_s(\mathbf{x}))$.

The governing equations driving the motion of fluid and structure written in the reference domains read as

$$\begin{cases} \rho_p \dfrac{\partial \mathbf{v}_s}{\partial t} + \rho_f \dfrac{\partial \mathbf{q}}{\partial t} = J^{-1}\mathrm{div}\left(J(\sigma_p \circ \xi_s)\mathbf{F}^{-T}\right) & \text{in } \Omega_s \\ \rho_f \dfrac{\partial \mathbf{v}_s}{\partial t} + \dfrac{\rho_f}{\varphi}\dfrac{\partial \mathbf{q}}{\partial t} = -K^{-1}\mathbf{q} - \mathbf{F}^{-T}\nabla p & \text{in } \Omega_s \\ \rho_f \dfrac{\partial \mathbf{v}_f}{\partial t} = J^{-1}\mathrm{div}\left(J(\sigma_f \circ \xi_f)\mathbf{F}^{-T}\right) - \rho_f \nabla\mathbf{v}_f \left(\mathbf{F}^{-1}\left(\mathbf{v}_f - \dfrac{\partial \mathbf{u}}{\partial t}\right)\right) & \text{in } \Omega_f \end{cases} \tag{1.14}$$

and the mass conservation reads as

$$\begin{cases} -s_0 \dfrac{\partial p_d}{\partial t} = \mathbf{F}^{-1} : \nabla(\mathbf{v}_s + \mathbf{q}) & \text{in } \Omega_s \\ \mathbf{F}^{-1} : \nabla\mathbf{v}_f = 0 & \text{in } \Omega_f \end{cases} \tag{1.15}$$

where for (1.15) we used $\mathrm{div}\,(J\mathbf{F}^{-1}\mathbf{v}) = J\nabla\mathbf{v} : \mathbf{F}^{-T}$ thanks to the Piola identity. The deformation of the structure can be found by integrating the kinematic equation

$$\frac{\partial \mathbf{u}_s}{\partial t} = \mathbf{v}_s \quad \text{in } \Omega_s. \tag{1.16}$$

The boundary and interface conditions are the same in the ALE formulation. The normal $\mathbf{n}$ (and projector $\mathbf{P} = \mathbf{I} - \mathbf{n}\mathbf{n}^T$) to the interface and outflow boundary in the physical domain can be computed from the reference normal $\widehat{\mathbf{n}}$, i.e., $\mathbf{n} = \mathbf{F}^{-T}\widehat{\mathbf{n}}/|\mathbf{F}^{-T}\widehat{\mathbf{n}}|$. Further, we will use the identities $J\,\mathrm{d}\widehat{x} = \mathrm{d}x$, $J|\mathbf{F}^{-T}\widehat{\mathbf{n}}|\,\mathrm{d}\widehat{s} = \mathrm{d}s$, where $\mathrm{d}s$ and $\mathrm{d}\widehat{s}$ are elementary areas orthogonal to $\mathbf{n}$ and $\widehat{\mathbf{n}}$ in the physical and reference coordinates, respectively. We collect all conditions in one place here:

$$\mathbf{v}_f = \mathbf{g} \ \text{ on } \Gamma_{f0}, \quad \sigma_f\mathbf{n} = \mathbf{0} \ \text{ on } \Gamma_{\mathrm{out}}, \quad \sigma_p\mathbf{n} = \mathbf{0} \ \text{ on } \Gamma_{s0}, \quad p_d = 0 \ \text{ on } \Gamma_{s0} \tag{1.17}$$

for the outer boundaries and

$$\sigma_f \mathbf{n} = \sigma_p \mathbf{n}, \qquad \mathbf{n}^T \sigma_f \mathbf{n} = -p_d + \frac{\rho_f}{2}|\mathbf{v}_f|^2 \quad \text{on } \Gamma_{fs} \tag{1.18}$$

$$\mathbf{v}_f \cdot \mathbf{n} = (\mathbf{v}_s + \mathbf{q}) \cdot \mathbf{n} \quad \text{on } \Gamma_{fs} \tag{1.19}$$

$$\mathbf{P}\sigma_f \mathbf{n} = -\gamma \mathbf{P} K^{-1/2}(\mathbf{v}_f - \mathbf{v}_s) \quad \text{on } \Gamma_{fs} \tag{1.20}$$

for the interface.

The constitutive relation for the Newtonian fluid in the reference domain reads

$$\sigma_f = -p_f \mathbf{I} + \mu_f(\nabla \mathbf{v} \mathbf{F}^{-1} + \mathbf{F}^{-T}(\nabla \mathbf{v})^T) \quad \text{in } \Omega_f. \tag{1.21}$$

For the structure we consider the compressible geometrically nonlinear SVK material with

$$\sigma_s = J^{-1}\mathbf{F}\mathbf{S}\mathbf{F}^T, \quad \mathbf{S} = \lambda_s \mathrm{tr}(\mathbf{E})\mathbf{I} + 2\mu_s \mathbf{E} \tag{1.22}$$

where $\mathbf{E} = \frac{1}{2}\left(\mathbf{F}^T\mathbf{F} - \mathbf{I}\right)$ is the Lagrange–Green strain tensor and λ_s, μ_s are the Lame constants.

Thus, the FPSI problem in the reference coordinates consists in finding pressure distributions p_d, p_f, fluid and structure velocity fields $\mathbf{v}_f$, $\mathbf{v}_s$, fluid flux in the porous medium $\mathbf{q}$ and the displacement field $\mathbf{u}$ satisfying the set of equations, interface and boundary conditions (1.14)–(1.20), together with (1.21), (1.22), and subject to a given extension rule (1.13).

2. Discretization

We now proceed with discretization of the FPSI problem formulated in the reference domain. Treating the problem in the reference domain allows us to avoid time-dependent triangulations and finite element function spaces and apply the standard method of lines to decouple space and time discretizations. We adopt a finite element method in space and define a consistent triangulation of the reference domain $\overline{\Omega}(0)$ as a collection $\mathscr{T}_h$ of shape-regular tetrahedra such that the triangulation respects the interface Γ_{fs}. This implies that $\mathscr{T}_h^a := \{T \in \mathscr{T}_h : T \subset \Omega_a\}$, $a \in \{f,s\}$, are consistent triangulations of the fluid and poroelastic reference domains Ω_a, $a \in \{f,s\}$. We consider the finite element Taylor–Hood spaces which are popular for simulation of incompressible fluid flow:

$$\mathbb{V}_h^a = \{\mathbf{v} \in C(\Omega_a) : \mathbf{v}|_T \in P_2(T)^3 \quad \forall T \in \mathscr{T}_h^a\}, \quad a \in \{f,s\}$$
$$\mathbb{Q}_h^a = \{q \in C(\Omega_a) : q|_T \in P_1(T) \quad \forall T \in \mathscr{T}_h^a\}, \quad a \in \{f,s\}.$$

For trial functions we need also the following subspaces:

$$\mathbb{V}_h^{f,0} = \{\mathbf{v} \in \mathbb{V}_h^f : \mathbf{v}|_{\Gamma_{f,0}} = \mathbf{0}\}$$
$$\mathbb{Q}_h^{s,0} = \{q \in \mathbb{Q}_h^s : q|_{\Gamma_{s,0}} = 0\}.$$

Note that the Taylor–Hood element is not a standard Darcy element for $H(\mathrm{div})$- formulations of the problem. In particular, it fails to provide elementwise mass conservation. However, for applications where the local mass conservation is not a major concern, it is a legitimate choice leading to the first order convergence in the Darcy region in product L^2-velocity–H^1-pressure norm [24], which is optimal for this pair of norms.

For the time discretization, we assume a constant time step Δt and use the notation $f^k(\mathbf{x}) \approx f(k\Delta t, \mathbf{x})$ for all time-dependent quantities.

To make the discretization energy-consistent, we note that the mass conservation law yields $J_t + \mathrm{div}\left(J\mathbf{F}^{-1}(\mathbf{v}_f - \mathbf{u}_t)\right) = 0$ in Ω_f. With the help of this identity and $\sqrt{J}(\sqrt{J})_t = \frac{1}{2}J_t$, the last equation in (1.14) can be re-written as follows:

$$\begin{aligned}\sqrt{J}\rho_f \frac{\partial(\sqrt{J}\mathbf{v}_f)}{\partial t} =& \mathrm{div}\left(J(\sigma_f \circ \xi_f)\mathbf{F}^{-T}\right) - \rho_f J \nabla \mathbf{v}_f \left(\mathbf{F}^{-1}\left(\mathbf{v}_f - \frac{\partial \mathbf{u}}{\partial t}\right)\right) \\ &- \frac{\rho_f}{2}\mathrm{div}\left(J\mathbf{F}^{-1}\left(\mathbf{v}_f - \frac{\partial \mathbf{u}}{\partial t}\right)\right)\mathbf{v}_f. \end{aligned} \tag{2.1}$$

The reformulation is similar to the one suggested in [21] to build an energy conserving scheme for the Eulerian form of the incompressible Navier–Stokes equations with variable density. In physical domain (i.e., $\mathbf{u} = 0$, $\mathbf{F} = \mathbf{I}$) the last two terms reduce to $\rho_f\big((\mathbf{v}_f \cdot \nabla)\mathbf{v}_f + \frac{1}{2}(\mathrm{div}\,\mathbf{v}_f)\mathbf{v}_f\big)$, which is well known to ensure energy conservation on the discrete level for weakly divergence free solutions (see, e.g., [13]). We will use (2.1) to formulate a finite element method below.

We proceed to multi-linear forms needed for our finite element formulation. For time derivatives, we need the form:

$$\begin{aligned} m^k(\mathbf{w}_s, \mathbf{w}_d, \mathbf{w}_f, r; \psi_s, \psi_d, \psi_f, q) :=& \int_{\Omega_s} J^{k-1}(\rho_p \mathbf{w}_s + \rho_f \mathbf{w}_d)\psi_s \,\mathrm{d}x \\ &+ \int_{\Omega_s}\left(\rho_f \mathbf{w}_s + \frac{\rho_f}{\varphi}\mathbf{w}_d\right)\psi_d \,\mathrm{d}x + \int_{\Omega_s} s_0 r q \,\mathrm{d}x \\ &+ \int_{\Omega_f} \rho_f \sqrt{J^{k-1}}\mathbf{w}_f \psi_f \,\mathrm{d}x. \end{aligned}$$

In the porous structure we define

$$a_d^k(\mathbf{w}_d, \psi_s) = \int_{\Omega_s} K^{-1}\mathbf{w}_d \cdot \psi_d \,\mathrm{d}x.$$

To handle SVK material, we define

$$a_s^k(\mathbf{w}_s, \psi_s) = \int_{\Omega_s} \mathbf{F}_{k-1}\mathbf{S}(\mathbf{w}_s, \mathbf{u}^{k-1}) : \nabla \psi_s \,\mathrm{d}x$$

where $\mathbf{F}_{k-1} := \mathbf{F}(\mathbf{u}^{k-1})$, $\mathbf{S}(\mathbf{u}_1, \mathbf{u}_2) := \lambda_s \mathrm{tr}(\mathbf{E}(\mathbf{u}_1, \mathbf{u}_2))\mathbf{I} + 2\mu_s \mathbf{E}(\mathbf{u}_1, \mathbf{u}_2)$, $\mathbf{E}(\mathbf{u}_1, \mathbf{u}_2) := \frac{1}{2}\left\{\mathbf{F}(\mathbf{u}_1)^T\mathbf{F}(\mathbf{u}_2) - \mathbf{I}\right\}_s$. Here and further $\{\mathbf{A}\}_s = \frac{1}{2}(\mathbf{A} + \mathbf{A}^T)$ denotes the symmetric part of tensor $\mathbf{A} \in \mathbb{R}^{3\times 3}$.

For the fluid domain we need the form for the viscous terms:

$$a_f^k(\mathbf{w}_f, \boldsymbol{\psi}_f) = \int_{\Omega_f} 2\mu_f J^{k-1} \mathbf{D}_{\mathbf{u}^{k-1}}(\mathbf{w}_f) : \mathbf{D}_{\mathbf{u}^{k-1}}(\boldsymbol{\psi}_f)\,\mathrm{d}x$$

where $\mathbf{D}_{\mathbf{u}}(\mathbf{v}) := \{(\nabla \mathbf{v})\mathbf{F}^{-1}(\mathbf{u})\}_s$, and the form for the inertia terms as they appear in (2.1):

$$\begin{aligned} &c_f^k(\mathbf{w}_f; \boldsymbol{\varphi}_f, \boldsymbol{\psi}_f) \\ &\quad = \int_{\Omega_f} \rho_f J^{k-1} \left(\nabla \mathbf{w}_f \mathbf{F}_{k-1}^{-1} \boldsymbol{\varphi}_f\right) \cdot \boldsymbol{\psi}_f \,\mathrm{d}x + \int_{\Omega_f} \frac{\rho_f}{2} \mathrm{div}\left(J^{k-1} \mathbf{F}_{k-1}^{-1} \boldsymbol{\varphi}_f\right) \mathbf{w}_f \cdot \boldsymbol{\psi}_f \,\mathrm{d}x. \end{aligned}$$

For handling the mass conservation constraints, we introduce

$$b_f^k(q, \boldsymbol{\psi}) = \int_{\Omega_f} q \mathbf{F}_{k-1}^{-T} : \nabla \boldsymbol{\psi}\,\mathrm{d}x, \quad b_s^k(q, \boldsymbol{\psi}) = \int_{\Omega_s} q \mathbf{F}_{k-1}^{-T} : \nabla \boldsymbol{\psi}\,\mathrm{d}x.$$

Next, we collect interface terms as they appear in the integral formulation (1.8):

$$\begin{aligned} d^k(\mathbf{w}_s, \mathbf{w}_d, \mathbf{w}_f, p_d; \boldsymbol{\psi}_s, \boldsymbol{\psi}_d, \boldsymbol{\psi}_f) = \gamma &\int_{\Gamma_{fs}} J_s^{k-1}\, K^{-1/2} \left(\mathbf{P}(\mathbf{w}_f - \mathbf{w}_s)\right) \cdot \left(\mathbf{P}(\boldsymbol{\psi}_f - \boldsymbol{\psi}_s)\right) \mathrm{d}s \\ &+ \int_{\Gamma_{fs}} J_s^{k-1} p_d (\boldsymbol{\psi}_f - \boldsymbol{\psi}_s - \boldsymbol{\psi}_d) \cdot \mathbf{n}\,\mathrm{d}s \\ &+ \int_{\Gamma_{fs}} J_s^{k-1} \frac{\rho_f}{2} |\mathbf{w}_f|^2 (\boldsymbol{\psi}_s - \boldsymbol{\psi}_f) \cdot \mathbf{n}\,\mathrm{d}s \end{aligned}$$

with $\mathbf{n} = \mathbf{F}_{k-1}^{-T}\widehat{\mathbf{n}}/|\mathbf{F}_{k-1}^{-T}\widehat{\mathbf{n}}|$, $\mathbf{P} = \mathbf{I} - \mathbf{n}\mathbf{n}^T$, and $J_s^{k-1} := J^{k-1}|\mathbf{F}_{k-1}^{-T}\widehat{\mathbf{n}}|$. We introduce the penalty term to enforce the continuity of normal flux condition (1.19):

$$\begin{aligned} &s^k(\mathbf{w}_s, \mathbf{w}_d, \mathbf{w}_f; \boldsymbol{\psi}_s, \boldsymbol{\psi}_d, \boldsymbol{\psi}_f, q_d) \\ &\qquad = \tau \int_{\Gamma_{fs}} J_s^{k-1} \left((\mathbf{w}_f - \mathbf{w}_s - \mathbf{w}_d)^T \mathbf{n}\right) \left((\boldsymbol{\psi}_f - \boldsymbol{\psi}_s - \boldsymbol{\psi}_d)^T \mathbf{n}\right) \mathrm{d}s \\ &\qquad\quad - \varkappa \int_{\Gamma_{fs}} J_s^{k-1} q_d (\mathbf{w}_f - \mathbf{w}_s - \mathbf{w}_d) \cdot \mathbf{n}\,\mathrm{d}s, \quad \varkappa \in \{0, 1\}. \end{aligned}$$

Parameter τ is a penalty parameter. Letting $\tau \gg 1$ forces the finite element solution to satisfy (approximately) the normal velocity continuity condition. Since Γ_{fs} is fitted by the mesh, taking τ arbitrary large does not cause locking. For $\varkappa = 1$ the last term is consistent (since it vanishes if $\mathbf{w}_s$ represents velocities of the true solution) and it skew-symmetrizes the pressure-dependent interface term. One can see that the scheme is energy consistent for both $\varkappa = 0$ and $\varkappa = 1$. We note that for unfitted interfaces the Nitsche method for the weak enforcement of the essential interface conditions may be more attractive [22]. The Nitsche method adds extra interface terms but in general allows relatively small τ, e.g., $\tau = O(h^{-1})$.

Denote by $[\partial f/\partial t]^k := (f^k - f^{k-1})/\Delta t$ the backward difference time. The finite element method reads: Given $\mathbf{u}^{k-1}$, $\mathbf{v}_f^{k-1}$, $\mathbf{v}_s^{k-1}$, $\mathbf{q}^{k-1}$, p_d^{k-1} find $\mathbf{v}_f^k \in \mathbb{V}_h^f$, $\mathbf{v}_s^k \in \mathbb{V}_h^s$, $\mathbf{q}^k \in \mathbb{V}_h^s$, $p_f^k \in \mathbb{Q}_h^f$, $p_d^k \in \mathbb{Q}_h^{s,0}$ such that $\mathbf{v}_f^k = \mathbf{g}_h(\cdot,(k)\Delta t)$ on Γ_{f0}, and it holds:

$$
\begin{aligned}
m^k\left(\left[\frac{\partial \mathbf{v}_s}{\partial t}\right]^k, \left[\frac{\partial \mathbf{q}}{\partial t}\right]^k, \left[\frac{\partial(\sqrt{J^{k-1}}\mathbf{v}_f)}{\partial t}\right]^k, \left[\frac{\partial p_d}{\partial t}\right]^k; \psi_s, \psi_d, \psi_f, q_d\right) \\
+ a_s^k(\mathbf{u}_s^k, \psi_s) + a_d(\mathbf{q}^k, \psi_s) + a_f^k(\mathbf{v}_f^k, \psi_f) + c_f^k\left(\mathbf{v}_f^k, \mathbf{v}_f^k - \left[\frac{\partial \mathbf{u}}{\partial t}\right]^k, \psi_f\right) \\
+ d^k(\mathbf{v}_s^k, \mathbf{q}^k, \mathbf{v}_f^k; \psi_s, \psi_d, \psi_f) + s^k(\mathbf{v}_s^k, \mathbf{q}^k, \mathbf{v}_f^k; \psi_s, \psi_d, \psi_f, q_d) \\
- b_s^k(p_d, \psi_s + \psi_d) - b_f^k(p_f, \psi_f) + b_s^k(q_d, \mathbf{v}_s^k + \mathbf{q}^k) + b_f^k(q_f, \mathbf{v}_f^k) = 0
\end{aligned}
\tag{2.2}
$$

for all $\psi_f \in \mathbb{V}_h^{f,0}$, $\psi_s \in \mathbb{V}_h^s$, $\psi_d \in \mathbb{V}_h^s$, $q_f \in \mathbb{Q}_h^f$, $q_d \in \mathbb{Q}_h^{s,0}$. In addition, we relate the finite element displacement and the velocity field in the porous structure through the kinematic equation

$$
\left[\frac{\partial \mathbf{u}}{\partial t}\right]^k = \mathbf{v}_s^k \quad \text{in } \Omega_s. \tag{2.3}
$$

Equations (2.2)–(2.3) subject to the initial conditions and an equation for continuous extension of $\mathbf{u}^k$ from Ω_s onto Ω_f define the discrete problem. In our implementation, the continuous extension of $\mathbf{u}$ in (1.13) is provided by the elasticity equation written for the velocity of the displacement [27]:

$$
\begin{aligned}
-\operatorname{div}\Bigg[J\Bigg(\lambda_m \operatorname{tr}\left(\nabla\left[\frac{\partial \mathbf{u}}{\partial t}\right]^k \mathbf{F}^{-1}\right)\mathbf{I} \\
+ \mu_m\left(\nabla\left[\frac{\partial \mathbf{u}}{\partial t}\right]^k \mathbf{F}^{-1} + \left(\nabla\left[\frac{\partial \mathbf{u}}{\partial t}\right]^k \mathbf{F}^{-1}\right)^T\right)\Bigg)\mathbf{F}^{-T}\Bigg] = 0 \quad \text{in } \Omega_f
\end{aligned}
\tag{2.4}
$$

satisfying the boundary condition $[\partial \mathbf{u}/\partial t]^k = \mathbf{v}^k$ on the interface Γ_{fs}. The space dependent elasticity parameters are $\mu_m = \mu_s|\Delta_e|^{-1.2}$, $\lambda_m = 16\mu_m$, where $|\Delta_e|$ denotes the physical volume of a mesh tetrahedron Δ_e subjected to displacement from the previous time step [27].

3. Numerical stability

In this section, we are interested in a stability estimate for the solution to (2.2)–(2.3). Similarly to the analysis of the dissipation property of the continuous problem, for the stability analysis we have to assume that the elastic porous material is incompressible. The Lagrangian mapping of Ω_s and the mass conservation yield $(\rho_s J)_t = 0$ and thus the assumption $\rho_s = \text{const}$ implies $J^k = 1$ in Ω_s for all k. We

consider the homogeneous boundary conditions on Γ_{f0}, i.e., $\mathbf{g}=\mathbf{0}$ in (1.17). Another important assumption is that the extension of deformation field from Ω_s to Ω_f defined in (2.4) does not degenerate or change the space orientation and so $J^k>0$ in Ω_f for all $k=1,2,\dots$. For the sake of notation let $\|f\|^2_{\Omega_f^k}:=\int_{\Omega_f}J^{k-1}f^2\,\mathrm{d}x$ and $\|f\|^2_{\Omega_a}:=\int_{\Omega_a}f^2\,\mathrm{d}x$, $a\in\{f,s\}$.

We further prove numerical stability of the method, which is explicit in all terms resulting from the geometry evolution. We allow $\varkappa\in\{0,1\}$.

We set $\psi_f=\mathbf{v}_f^k$, $\psi_s=\mathbf{v}_s^k$, $\psi_d=\mathbf{q}^k$, $q_d=p_d^k$ in (2.2). For the first bilinear form we use $\rho_p=\rho_s(1-\varphi)+\rho_f\varphi$ to re-organize

$$
\begin{aligned}
&m^k\left(\left[\frac{\partial\mathbf{v}_s}{\partial t}\right]^k,\left[\frac{\partial\mathbf{q}}{\partial t}\right]^k,\left[\frac{\partial(\sqrt{J^{k-1}}\mathbf{v}_f)}{\partial t}\right]^k,\left[\frac{\partial p_d}{\partial t}\right]^k;\mathbf{v}_s^k,\mathbf{q}^k,\mathbf{v}_f^k,p_d\right)\\
&\quad=\underbrace{\int_{\Omega_s}\left((1-\varphi)\rho_s\left[\tfrac{\partial\mathbf{v}_s}{\partial t}\right]^k\cdot\mathbf{v}_s^k+\varphi\rho_f\left[\tfrac{\partial(\mathbf{v}_s+\varphi^{-1}\mathbf{q})}{\partial t}\right]^k\cdot(\mathbf{v}_s^k+\varphi^{-1}\mathbf{q}^k)+s_0\left[\tfrac{\partial p_d}{\partial t}\right]^k p_d^k\right)\mathrm{d}x}_{=I_1}\\
&\qquad+\int_{\Omega_f}\rho_f\left[\frac{\partial(\sqrt{J^{k-1}}\mathbf{v}_f)}{\partial t}\right]^k\sqrt{J^{k-1}}\mathbf{v}_f^k\,\mathrm{d}x.
\end{aligned}
\tag{3.1}
$$

The polarization identity, $(b-a)b=\frac{1}{2}(b^2-a^2+(b-a)^2)$ gives for I_1-term:

$$
\begin{aligned}
I_1=&\frac{(1-\varphi)\rho_s}{2\Delta t}\left(\|\mathbf{v}_s^k\|^2_{\Omega_s}-\|\mathbf{v}_s^{k-1}\|^2_{\Omega_s}\right)+\frac{s_0}{2\Delta t}\left(\|p_d^k\|^2_{\Omega_s}-\|p_d^{k-1}\|^2_{\Omega_s}\right)\\
&+\frac{\varphi\rho_f}{2\Delta t}\left(\|\mathbf{v}_s^k+\varphi^{-1}\mathbf{q}^k\|^2_{\Omega_s}-\|\mathbf{v}_s^{k-1}+\varphi^{-1}\mathbf{q}^{k-1}\|^2_{\Omega_s}\right)\\
&+\frac{|\Delta t|}{2}\left((1-\varphi)\rho_s\left\|\left[\frac{\partial\mathbf{v}_s}{\partial t}\right]^k\right\|^2_{\Omega_s}+\varphi\rho_f\left\|\left[\frac{\partial(\mathbf{v}_s+\varphi^{-1}\mathbf{q})}{\partial t}\right]^k\right\|^2_{\Omega_s}+s_0\left\|\left[\frac{\partial p_d}{\partial t}\right]^k\right\|^2_{\Omega_s}\right).
\end{aligned}
$$

For the last term in (3.1) we get

$$
\begin{aligned}
\int_{\Omega_f}\rho_f\left[\frac{\partial(\sqrt{J^{k-1}}\mathbf{v}_f)}{\partial t}\right]^k\sqrt{J^{k-1}}\mathbf{v}_f^k\,\mathrm{d}x=&\frac{\rho_f}{2\Delta t}\left(\left\|\sqrt{J^{k-1}}\mathbf{v}_f^k\right\|^2_{\Omega_f}-\left\|\sqrt{J^{k-2}}\mathbf{v}_f^{k-1}\right\|^2_{\Omega_f}\right)\\
&+\frac{|\Delta t|\,\rho_f}{2}\left\|\left[\frac{\partial(\sqrt{J^{k-1}}\mathbf{v}_f)}{\partial t}\right]^k\right\|^2_{\Omega_f}.
\end{aligned}
\tag{3.2}
$$

The c_f-form term vanishes due to the skew-symmetry of the form. For the treatment

of elastic term we note the identities:

$$\begin{aligned}2\Big(\mathbf{E}(\mathbf{u}^{k-1},\mathbf{u}^k)-\mathbf{E}(\mathbf{u}^{k-2},\mathbf{u}^{k-1})\Big) &= \{\mathbf{F}_{k-1}^T\mathbf{F}_k\}_s - \{\mathbf{F}_{k-2}^T\mathbf{F}_{k-1}\}_s\\ &= \{\mathbf{F}_{k-1}^T\mathbf{F}_k\}_s - \{\mathbf{F}_{k-1}^T\mathbf{F}_{k-2}\}_s\\ &= \{\mathbf{F}_{k-1}^T(\mathbf{F}_k-\mathbf{F}_{k-2})\}_s\\ &= \{\mathbf{F}_{k-1}^T(\nabla\mathbf{u}^k-\nabla\mathbf{u}^{k-2})\}_s. \end{aligned} \tag{3.3}$$

Hence due to the symmetry of $\mathbf{S}$ it holds

$$\begin{aligned}&\mathbf{F}_{k-1}\mathbf{S}(\mathbf{u}^k,\mathbf{u}^{k-1}) : (\nabla\mathbf{u}^k-\nabla\mathbf{u}^{k-2})\\ &\qquad = \mathbf{S}(\mathbf{u}^k,\mathbf{u}^{k-1}) : \{\mathbf{F}_{k-1}^T(\nabla\mathbf{u}^k-\nabla\mathbf{u}^{k-2})\}_s\\ &\qquad = 2\mathbf{S}(\mathbf{u}^k,\mathbf{u}^{k-1}) : (\mathbf{E}(\mathbf{u}^{k-1},\mathbf{u}^k)-\mathbf{E}(\mathbf{u}^{k-2},\mathbf{u}^{k-1})).\end{aligned} \tag{3.4}$$

The discrete elastic energy is defined by

$$\mathscr{E}_k := \int_{\Omega_s}\frac{\lambda_s}{2}\Big[\mathrm{tr}(\mathbf{E}(\mathbf{u}^{k-1},\mathbf{u}^k))\Big]^2+\mu_s\left|\mathbf{E}(\mathbf{u}^{k-1},\mathbf{u}^k)\right|_F^2\,\mathrm{d}x.$$

Thanks to (3.3) and (3.4) we obtain for the elasticity term in (2.2):

$$\begin{aligned}a_s^k(\mathbf{u}_s^k,\mathbf{v}_s^k) &= \int_{\Omega_s}\mathbf{F}_{k-1}\mathbf{S}(\mathbf{u}^k,\mathbf{u}^{k-1}) : \nabla\mathbf{v}_s^k\,\mathrm{d}x = \int_{\Omega_s}\mathbf{F}_{k-1}\mathbf{S}(\mathbf{u}^k,\mathbf{u}^{k-1}) : \nabla\left[\frac{\partial\mathbf{u}}{\partial t}\right]^k\mathrm{d}x\\ &= \frac{1}{\Delta t}\int_{\Omega_s}\mathbf{S}(\mathbf{u}^k,\mathbf{u}^{k-1}) : (\mathbf{E}(\mathbf{u}^{k-1},\mathbf{u}^k)-\mathbf{E}(\mathbf{u}^{k-2},\mathbf{u}^{k-1}))\,\mathrm{d}x\\ &= \frac{1}{\Delta t}(\mathscr{E}_k-\mathscr{E}_{k-1})\\ &\quad+\Delta t\int_{\Omega_s}\frac{\lambda_s}{2}\left|\left[\frac{\partial\mathrm{tr}(\mathbf{E}(\widetilde{\mathbf{u}},\mathbf{u}))}{\partial t}\right]^k\right|^2+\mu_s\left|\left[\frac{\partial\mathbf{E}(\widetilde{\mathbf{u}},\mathbf{u})}{\partial t}\right]^k\right|_F^2\mathrm{d}x\end{aligned} \tag{3.5}$$

where $\widetilde{u}^k = u^{k-1}$.

Kinetic energy of elastic structure, Darcy fluid, and free stream fluid are defined as

$$\mathscr{K}_k^s = \frac{(1-\varphi)\rho_s}{2}\|\mathbf{v}_s^k\|_{\Omega_s}^2,\quad \mathscr{K}_k^d = \frac{\varphi\rho_f}{2}\|\mathbf{v}_s^k+\varphi^{-1}\mathbf{q}^k\|_{\Omega_s}^2,\quad \mathscr{K}_k^f = \frac{\rho_f}{2}\|\mathbf{v}_f^k\|_{\Omega_f^k}^2.$$

With this notation, the energy balance of the discrete method reads:

$$\underbrace{\frac{1}{\Delta t}\left([\mathscr{K}_k^s+\mathscr{K}_k^d+\mathscr{K}_k^f+\mathscr{E}_k]-[\mathscr{K}_{k-1}^s+\mathscr{K}_{k-1}^d+\mathscr{K}_{k-1}^f+\mathscr{E}_{k-1}]\right)+\frac{s_0}{2\Delta t}\left(\|p_d^k\|_{\Omega_s}^2-\|p_d^{k-1}\|_{\Omega_s}^2\right)}_{\text{variation of kinetic and free energy}}$$
$$\underbrace{+2\mu_f\|\mathbf{D}_{\mathbf{u}^{k-1}}(\mathbf{v}_f^k)\|_{\Omega_f^k}^2+\|K^{-1/2}\mathbf{q}^k\|_{\Omega_s}^2+\gamma\int_{\Gamma_{fs}}K^{-1/2}\left|\mathbf{P}(\mathbf{v}_f^k-\mathbf{v}_s^k)\right|^2\,\mathrm{d}s}_{\text{model dissipation}}$$
$$\underbrace{+\tau\int_{\Gamma_{fs}}\left|(\mathbf{v}_f^k-\mathbf{q}^k-\mathbf{v}_s^k)\cdot\mathbf{n}\right|^2\,\mathrm{d}s}_{\text{penalty for violating (1.19)}}+(1-\varkappa)\underbrace{\int_{\Gamma_{fs}}p_d^k(\mathbf{v}_f^k-\mathbf{q}^k-\mathbf{v}_s^k)\cdot\mathbf{n}\,\mathrm{d}s}_{\text{sign indefinite term}}+\mathscr{D}_k=0 \tag{3.6}$$

where $O(\Delta t)$ numerical dissipation terms are

$$\mathscr{D}_k:=\frac{\Delta t}{2}\left((1-\varphi)\rho_s\left\|\left[\frac{\partial\mathbf{v}_s}{\partial t}\right]^k\right\|_{\Omega_s}^2+\varphi\rho_f\left\|\left[\frac{\partial(\mathbf{v}_s+\varphi^{-1}\mathbf{q})}{\partial t}\right]^k\right\|_{\Omega_s}^2+s_0\left\|\left[\frac{\partial p_d}{\partial t}\right]^k\right\|_{\Omega_s}^2\right.$$
$$\left.+\rho_f\left\|\left[\frac{\partial(\sqrt{J^{k-1}}\mathbf{v}_f)}{\partial t}\right]^k\right\|_{\Omega_f}^2+\lambda_s\left\|\left[\frac{\partial\mathrm{tr}(\mathbf{E}(\widetilde{\mathbf{u}},\mathbf{u}))}{\partial t}\right]^k\right\|_{\Omega_s}^2+2\mu_s\left\|\left[\frac{\partial\mathbf{E}(\widetilde{\mathbf{u}},\mathbf{u})}{\partial t}\right]^k\right\|_{\Omega_s}^2\right).$$

For $\varkappa=1$ the discrete energy balance again mimics a continuous problem balance up to the penalty and $\mathscr{D}_k$ terms. These terms are positive, so the numerical scheme is dissipative.

One can show that for sufficiently large penalty parameter τ, this first order in time scheme is dissipative also for $\varkappa=0$ (no skew-symmetrization is added to the penalty in the definition of the s^k form). For this purpose, we also assume that the mesh near Γ_{fs} is quasi-uniform with characteristic mesh size h. To handle the extra interface term, we apply the Cauchy–Schwarz inequality:

$$\begin{aligned}\tau\int_{\Gamma_{fs}}\left|(\mathbf{v}_f^k-\mathbf{q}^k-\mathbf{v}_s^k)\cdot\mathbf{n}\right|^2\,\mathrm{d}s+\int_{\Gamma_{fs}}p_d^k(\mathbf{v}_f^k-\mathbf{q}^k-\mathbf{v}_s^k)\cdot\mathbf{n}\,\mathrm{d}s\\ \geqslant\frac{\tau}{2}\int_{\Gamma_{fs}}\left|(\mathbf{v}_f^k-\mathbf{q}^k-\mathbf{v}_s^k)\cdot\mathbf{n}\right|^2\,\mathrm{d}s-\frac{1}{2\tau}\int_{\Gamma_{fs}}|p_d^k|^2\,\mathrm{d}s\end{aligned} \tag{3.7}$$

and further estimate it using the FE trace inequality:

$$\begin{aligned}\frac{1}{2\tau}\int_{\Gamma_{fs}}|p_d^k|^2\,\mathrm{d}s\leqslant\frac{1}{2\tau}\int_{\Gamma_{fs}}|p_d^k|^2\,\mathrm{d}s\leqslant\frac{C}{h\tau}\|p_d^k\|_{\Omega_s}^2\\ \leqslant\frac{C}{h\tau}\left(\|p_d^0\|_{\Omega_s}^2+T\sum_{j=1}^k\Delta t\left\|\left[\frac{\partial p_d}{\partial t}\right]^j\right\|_{\Omega_s}^2\right)\leqslant\frac{C}{h\tau}\left(\|p_d^0\|_{\Omega_s}^2+2T\sum_{j=1}^k s_0^{-1}\mathscr{D}_j\right).\end{aligned}$$

Summing up for $k = 1, \dots, K$, with $K\Delta t \leqslant T$ we have

$$\sum_{k=1}^{K} \frac{1}{2\tau} \int_{\Gamma_{fs}} |p_d^k|^2 \, \mathrm{d}s \leqslant \frac{CT}{h\Delta t\, \tau} \left(\|p_d^0\|_{\Omega_s}^2 + 2T \sum_{j=1}^{K} s_0^{-1} \mathscr{D}_j \right). \tag{3.8}$$

We now scale (3.6) with Δt and sum up for $k = 1, \dots, K$. Omitting some positive terms on the left-hand side, and applying (3.7)–(3.8) to estimate the sign-indefinite term for $\varkappa = 0$, we get the energy stability estimate for the finite element solution:

$$\begin{aligned}
&\mathscr{K}_K^s + \mathscr{K}_K^d + \mathscr{K}_K^f + \mathscr{E}_K + \frac{s_0}{2} \|p_d^K\|_{\Omega_s}^2 \\
&\quad + \sum_{k=1}^{K} \Delta t \left\{ 2\mu_f \|\mathbf{D}_{\mathbf{u}^{k-1}}(\mathbf{v}_f^k)\|_{\Omega_f^k}^2 + \|K^{-1/2}\mathbf{q}^k\|_{\Omega_s}^2 + \gamma \int_{\Gamma_{fs}} K^{-1/2} \left| \mathbf{P}(\mathbf{v}_f^k - \mathbf{v}_s^k) \right|^2 \mathrm{d}s \right\} \\
&\quad \leqslant \mathscr{K}_0^s + \mathscr{K}_0^d + \mathscr{K}_0^f + \mathscr{E}_0 + \frac{s_0}{2} \|p_d^0\|_{\Omega_s}^2 + (1-\varkappa) C \|p_d^0\|_{\Omega_s}^2
\end{aligned} \tag{3.9}$$

where for $\varkappa = 0$ we choose the penalty parameter τ sufficiently large to satisfy

$$\tau \geqslant \frac{CT^2}{h\Delta t s_0}.$$

Here C is a positive constant that may depend on the shape regularity of the mesh, but not on the discretization parameters.

4. Numerical experiments

In this section we assess the performance of the proposed monolithic FPSI FE method. As the test problem we consider the propagation of a pressure impulse in a compliant tube with a porous wall filled with fluid. The problem setting follows the benchmark suggested in [17] for flow in a tube with an impermeable hyperelastic wall. The original problem is related to the blood flow through an artery. It has been extensively considered in the literature for validating the performance of FSI solvers [15, 16, 18, 19, 26, 31]. Since the test is an idealization of a practical setup, no experimental data is available and the test serves to validate mesh convergence and study physical plausibility of the computed solution.

The problem configuration consists of incompressible viscous flow through a poroelastic tube with circular cross-section. The tube is 50 mm long, it has inner radius 5mm and the wall thickness is 1mm. The fluid density is 10^{-3}g/mm^3 and kinematic viscosity is 3mm^2/s. The wall density ρ_s is $1.2 \cdot 10^{-3}$g/mm^3. In (1.22), the SVK hyperelastic model is used with elastic modulus $E = 3 \cdot 10^5 \mathrm{g}/(\mathrm{mm} \cdot \mathrm{s}^2)$ and Poisson's ratio $\nu = 0.3$. Initially, the fluid is at rest and the tube is non-deformed. The tube is fixed at both ends.

For the porous media parameters, we used porosity $\varphi = 0.3$ [14], mass storativity $s_0 = 5 \cdot 10^{-5} \mathrm{mm} \cdot \mathrm{s}^2/\mathrm{g}$ and two cases of the scalar permeability coefficient:

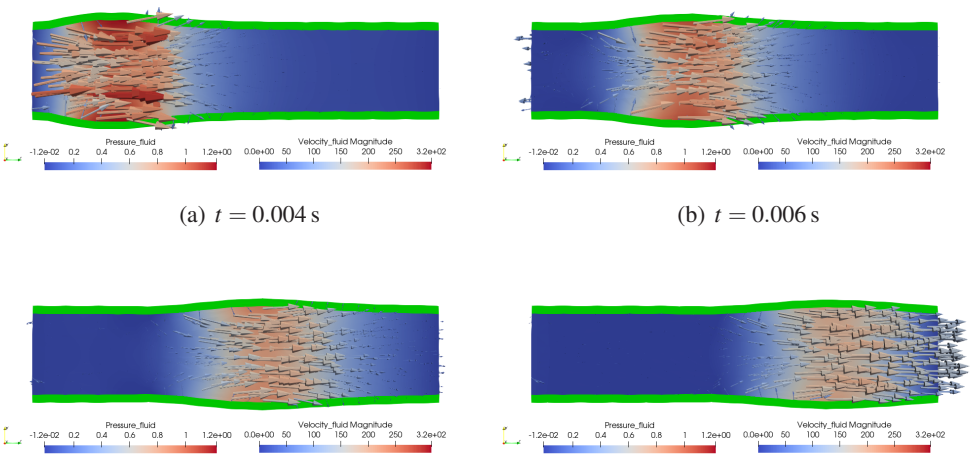

(a) $t = 0.004$ s (b) $t = 0.006$ s

(c) $t = 0.008$ s (d) $t = 0.01$ s

Figure 2. Pressure wave: middle cross-section velocity field, pressure distribution, velocity vectors and 10 times enlarged structure displacement for several time instances.

$K = 10^{-12}\text{mm}^2 = 10^{-18}\text{m}^2$ and $K = 10^{-5}\text{mm}^2 = 10^{-11}\text{m}^2$. The smaller value mimics permeability estimated in rat's cardiovascular system [14], while the larger value is taken artificially large.

On the left open boundary of the tube, the external pressure p_{ext} is set to $1.333 \cdot 10^3$Pa for $t \in (0, 3 \cdot 10^{-3})$ s and zero afterwards, while on the right open boundary the external pressure p_{ext} is zero throughout the experiment. This generates a pressure impulse that travels along the tube. The external pressure is incorporated into (2.2)–(2.3) through the open boundary condition $\sigma_f \mathbf{F}^{-T}\mathbf{n} = p_{\text{ext}}\mathbf{n}$.

We use the Taylor–Hood P2-P1 elements for velocity and pressure variables and P2 elements for displacements, with the first order semi-implicit Euler discretization. The scheme (2.2)–(2.3) is implemented on the basis of the open source package Ani3D [28]. The important feature of equation (2.2) is linearization on each time step due to extrapolation of all geometric factors and the advection velocity from the previous time steps. The resulting linear system is solved by the multifrontal sparse direct solver MUMPS [3].

The consistent mesh used for the numerical experiment has 13200 and 7200 tetrahedra for the fluid and solid subdomains, respectively, yielding 355976 degrees of freedom. We set $\Delta t = 10^{-4}$s, $\gamma = \mu_f$, $\tau = 10^3 \cdot h^{-1}$, where h is the local mesh size.

Figure 2 depicts the computed fluid velocity field in the middle cross-section for large permeability case. No visible difference was spotted for small permeability case so we do not show it here. The wall displacement is exaggerated by a factor of 10 in the figure for clarity. The redder the color of the arrow is, the larger magnitude the velocity vector has.

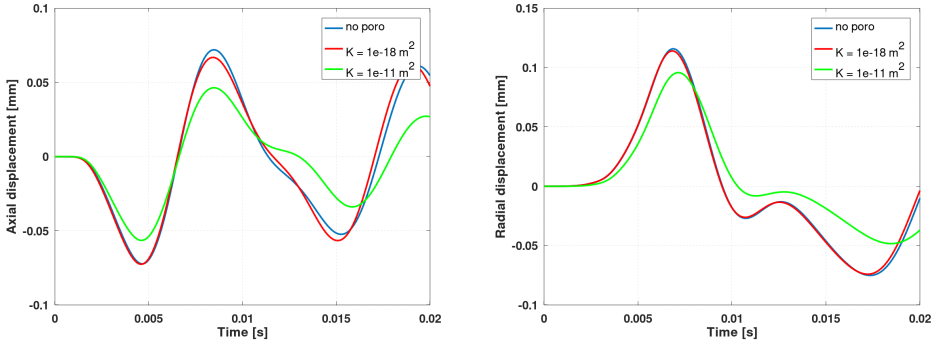

(a) axial component (b) radial component

Figure 3. The axial and radial components of displacement of the inner tube wall at half the length of the pipe. Solutions are shown for two cases of permeability and the pure FSI case (see the text).

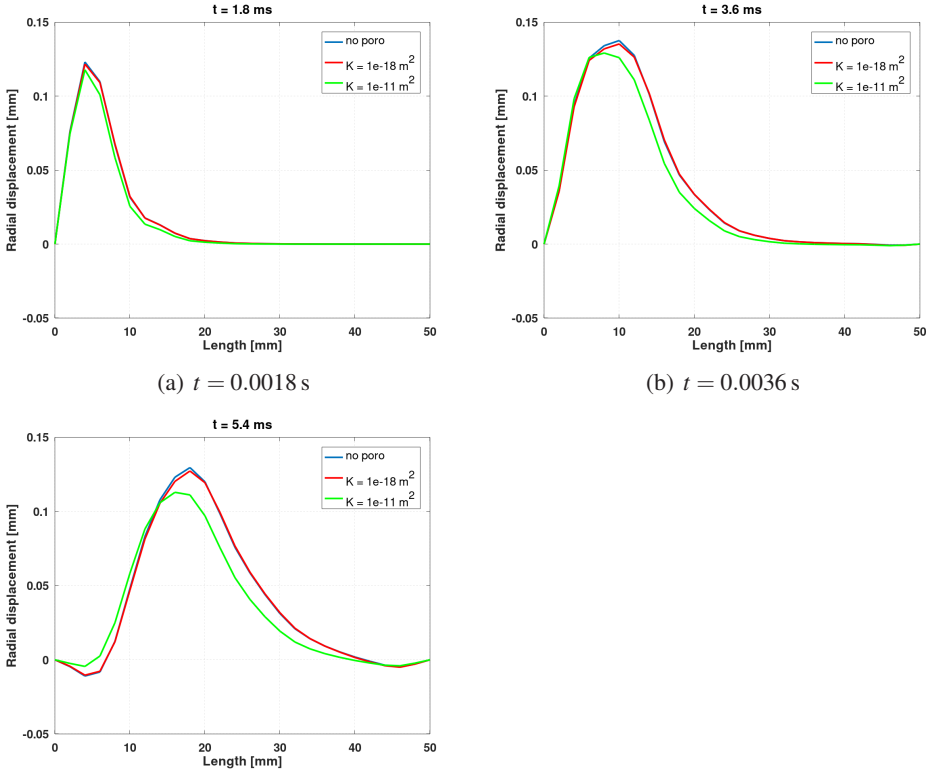

(a) $t = 0.0018\,\mathrm{s}$ (b) $t = 0.0036\,\mathrm{s}$

(c) $t = 0.0054\,\mathrm{s}$

Figure 4. Wall profile on the inner side along the tube length for several time instances.

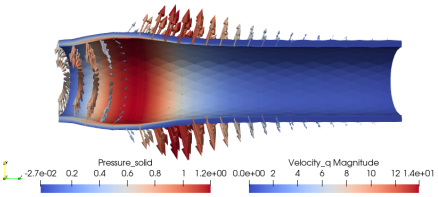

(a) $t = 0.004\,\mathrm{s}$

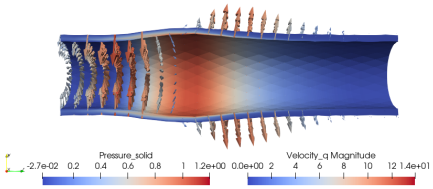

(b) $t = 0.006\,\mathrm{s}$

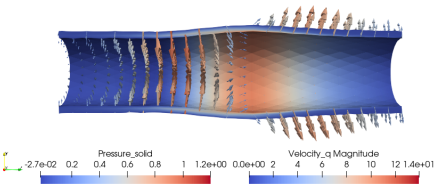

(c) $t = 0.008\,\mathrm{s}$

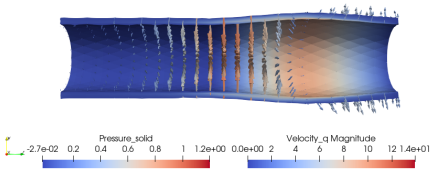

(d) $t = 0.01\,\mathrm{s}$

Figure 5. Porous pressure p_d and filtration velocity $\mathbf{q}$ distribution in the solid for $K = 10^{-5}\mathrm{mm}^2$: middle cross-section view, with 10 times enlarged structure displacement for several time instances.

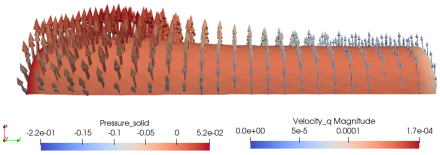

(a) $t = 0.004\mathrm{s}$

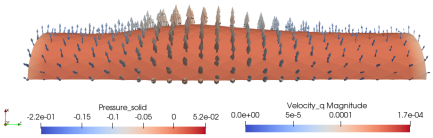

(b) $t = 0.006\mathrm{s}$

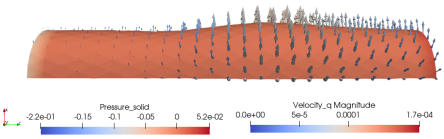

(c) $t = 0.008\mathrm{s}$

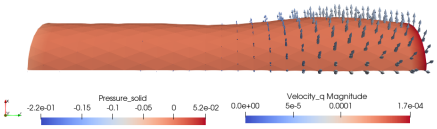

(d) $t = 0.01\mathrm{s}$

Figure 6. Porous pressure p_d and filtration velocity $\mathbf{q}$ distribution in the solid for $K = 10^{-12}\mathrm{mm}^2$: middle cross-section view, with 10 times enlarged structure displacement for several time instances.

Figure 3 shows the time variations of the radial and axial components of the displacement of the inner tube wall at half the length of the pipe, while Figure 4 shows the wall profile due to deformation at time instances $0.0018, 0.0036, 0.0054\mathrm{s}$. Both figures suggest that the smaller permeability case in this FPSI simulation scenario resembles the pure FSI case, which is an intuitively feasible result.

Figures 5 and 6 demonstrate the porous pressure and filtration velocity distributions for the same time instances as used in Fig. 2. According to the filtration velocity in Fig. 5, the fluid for the large permeability case tries to escape the tube wall in the exterior direction before the traveling inflection region while entering back into the wall past that region. For the small permeability, as seen on the legend of Fig. 6, the filtration velocity is predictably small.

References

1. C. Ager, B. Schott, M. Winter, and W. A. Wall, A Nitsche-based cut finite element method for the coupling of incompressible fluid flow with poroelasticity. *Computer Methods in Applied Mechanics and Engineering* **351** (2019), 253–280.

2. I. Ambartsumyan, E. Khattatov, I. Yotov, and P. Zunino, A Lagrange multiplier method for a Stokes–Biot fluid–poroelastic structure interaction model. *Numerische Mathematik* **140** (2018), No. 2, 513–553.

3. P. R. Amestoy et al., *MUMPS (MUltifrontal Massively Parallel sparse direct Solver)*. http://mumps-consortium.org

4. L. Badea, M. Discacciati, and A. Quarteroni, Numerical analysis of the Navier–Stokes/Darcy coupling. *Numerische Mathematik* **115** (2010), No 2, 195–227.

5. S. Badia, A. Quaini, and A. Quarteroni, Coupling Biot and Navier–Stokes equations for modelling fluid–poroelastic media interaction. *Journal of Computational Physics* **228** (2009), No. 21, 7986–8014.

6. Y. Bazilevs, J. R. Gohean, T. J. R. Hughes, R. D. Moser, and Y. Zhang, Patient-specific isogeometric fluid–structure interaction analysis of thoracic aortic blood flow due to implantation of the Jarvik 2000 left ventricular assist device. *Computer Methods in Applied Mechanics and Engineering* **198** (2009), No 45-46, 3534–3550.

7. M. Braack and P. B. Mucha, Directional do-nothing condition for the Navier–Stokes equations. *Journal of Computational Mathematics* (2014), 507–521.

8. M. Bukač, I. Yotov, R. Zakerzadeh, and P. Zunino, Partitioning strategies for the interaction of a fluid with a poroelastic material based on a Nitsches coupling approach. *Computer Methods in Applied Mechanics and Engineering* **292** (2015), 138–170.

9. M. Bukač, I. Yotov, R. Zakerzadeh, and P. Zunino, Effects of poroelasticity on fluid-structure interaction in arteries: A computational sensitivity study. In: *Modeling the Heart and the Circulatory System*. Springer, 2015.

10. A. Çeşmelioğlu and B. Rivière, Analysis of time-dependent Navier–Stokes flow coupled with Darcy flow. *Journal of Numerical Mathematics* **16** (2008), 249–280.

11. A. Cesmelioglu, V. Girault, and B. Riviere, Time-dependent coupling of Navier–Stokes and Darcy flows. *ESAIM: Mathematical Modelling and Numerical Analysis* **47** (2013), No. 2, 539–554.

12. A. Çeşmelioğlu and B. Rivière, Primal discontinuous Galerkin methods for time-dependent coupled surface and subsurface flow. *Journal of Scientific Computing* **40** (2009), No. 1, 115–140.

13. S. Charnyi, T. Heister, M. A. Olshanskii, and L. G. Rebholz, On conservation laws of Navier–Stokes Galerkin discretizations. *Journal of Computational Physics* **337** (2017), 289–308.

14. K. Y. Chooi, A. Comerford, S. J. Sherwin, and P. D. Weinberg, Intimal and medial contributions to the hydraulic resistance of the arterial wall at different pressures: a combined computational and experimental study. *Journal of The Royal Society Interface* **13** (2016), No. 119, 20160234.

15. J. Degroote, R. Haelterman, S. Annerel, P. Bruggeman, and J. Vierendeels, Performance of partitioned procedures in fluid–structure interaction. *Computers & Structures* **88** (2010), No. 7-8, 446–457.

16. A. Eken and M. Sahin, A parallel monolithic algorithm for the numerical simulation of large-scale fluid structure interaction problems. *International Journal for Numerical Methods in Fluids* **80** (2016), No. 12, 687–714.

17. L. Formaggia, J.-F. Gerbeau, F. Nobile, and A. Quarteroni, On the coupling of 3D and 1D Navier–Stokes equations for flow problems in compliant vessels. *Computer Methods in Applied Mechanics and Engineering* **191** (2001), No. 6-7, 561–582.

18. M. W. Gee, U. Küttler, and W. A. Wall, Truly monolithic algebraic multigrid for fluid–structure interaction. *International Journal for Numerical Methods in Engineering* **85** (2011), No. 8, 987–1016.

19. J.-F. Gerbeau and M. Vidrascu, A quasi-Newton algorithm based on a reduced model for fluid-structure interaction problems in blood flows. *ESAIM: Mathematical Modelling and Numerical Analysis* **37** (2003), No. 4, 631–647.

20. V. Girault and B. Rivière, DG approximation of coupled Navier–Stokes and Darcy equations by Beaver–Joseph–Saffman interface condition. *SIAM Journal on Numerical Analysis* **47** (2009), No. 3, 2052–2089.

21. J.-L. Guermond and L. Quartapelle, A projection FEM for variable density incompressible flows. *Journal of Computational Physics* **165** (2000), No. 1, 167–188.

22. A. Hansbo and P. Hansbo, An unfitted finite element method, based on Nitsches method, for elliptic interface problems. *Computer Methods in Applied Mechanics and Engineering* **191** (2002), No. 47-48, 5537–5552.

23. J. Hron and S. Turek, *A monolithic FEM/multigrid solver for an ALE formulation of fluid-structure interaction with applications in biomechanics*. Springer, Berlin–Heidelberg, 2006.

24. T. Karper, K.-A. Mardal, and R. Winther, Unified finite element discretizations of coupled Darcy–Stokes flow. *Numerical Methods for Partial Differential Equations: An International Journal* **25** (2009), No. 2, 311–326.

25. N. Koshiba, J. Ando, X. Chen, and T. Hisada, Multiphysics simulation of blood flow and LDL transport in a porohyperelastic arterial wall model. *Journal of Biomechanical Engineering* **129** (2007), No. 3, 374–385.

26. U. Küttler and W. A. Wall, Fixed-point fluid–structure interaction solvers with dynamic relaxation. *Computational Mechanics* **43** (2008), No. 1, 61–72.

27. M. Landajuela, M. Vidrascu, D. Chapelle, and M. A. Fernández, Coupling schemes for the FSI forward prediction challenge: comparative study and validation. *International Journal for Numerical Methods in Biomedical Engineering* **33** (2017), No. 4, e2813.

28. K. Lipnikov, Yu. Vassilevski, A. Danilov, et al., *Advanced Numerical Instruments 3D*. http://sourceforge.net/projects/ani3d

29. A. Lozovskiy, M. A. Olshanskii, V. Salamatova, and Yu. V. Vassilevski, An unconditionally stable semi-implicit FSI finite element method. *Computer Methods in Applied Mechanics and Engineering* **297** (2015), 437–454.

30. A. Lozovskiy, M. A. Olshanskii, and Yu. V. Vassilevski, Analysis and assessment of a monolithic FSI finite element method. *Computers & Fluids* **179** (2019), 277–288.

31. A. G. Malan and O. F. Oxtoby, An accelerated, fully-coupled, parallel 3D hybrid finite-volume fluid–structure interaction scheme. *Computer Methods in Applied Mechanics and Engineering* **253** (2013), 426–438.

32. T. J. Mitchison, G. T. Charras, and L. Mahadevan, Implications of a poroelastic cytoplasm for the dynamics of animal cell shape. In: *Seminars in Cell & Ddevelopmental Biology*, Vol. 19. Elsevier, 2008.

33. S. Polzer, T. C. Gasser, B. Markert, J. Bursa, and P. Skacel, Impact of poroelasticity of intraluminal thrombus on wall stress of abdominal aortic aneurysms. *Biomedical Engineering Online* **11** (2012), No. 1, 1–13.

34. R. Ruiz-Baier, M. Taffetani, H. D. Westermeyer, and I. Yotov, The Biot–Stokes coupling using total pressure: Formulation, analysis and application to interfacial flow in the eye. *Computer Methods in Applied Mechanics and Engineering* **389** (2022), 114384.

35. R. E. Showalter, Poroelastic filtration coupled to Stokes flow. *Lecture Notes in Pure and Applied Mathematics*, Vol. 242, 2005, 229.

36. J. Wen and Y. He, A strongly conservative finite element method for the coupled Stokes–Biot model. *Computers & Mathematics with Applications* **80** (2020), No. 5, 1421–1442.